

RESPONSE TO ANONYMOUS REVIEWER 3 COMMENTS

MS No.: angeo-2018-35

MS Type: Regular paper

Iteration: Minor Revision

MANUSCRIPT TITLE: **Solar Eclipse-Induced perturbations at mid-latitude during the 21 August 2017 event**

Dear Editor,

GENERAL RESPONSE

We thank the reviewer for the useful and supportive corrections/suggestions. We believed that all suggestions made have been attended to accordingly. Major corrections have been carried out and are highlighted (red colour) in the manuscript. More figures have been added as suggested, this has made the initial figure numbers to be reordered. The table has been edited to highlight the corresponding local time to the universal time of the solar eclipse progression. All additional references quoted in the text had been included in the reference list and highlighted in red colour.

Further, the names of the authors appears only because of their contributions in planing, data analysis and writing the report. Therefore, two more authors who participated largely in the review processes from the first submission to present have been added. The Authors list now reads “ *Bolarinwa J. Adekoya, Babatunde O. Adebisin, Victor. U. Chukwuma, Timothy W. David, Stephen O. Ikubanni, Shola J. Adebisi, and Olawale. S. Bolaji*” based on their contributions. The third author was/is my Ph.D supervisor/mentor who have contributed majorly to my academic growth till present. The last author is a senior colleague that rendered his help when we had problem in some key area during the revisions. Not only that, he partook in the general proofreading/editing of the manuscript.

The authors are grateful for the useful comments and suggestions on the structure of the manuscript. This has tremendously improved the standard of the manuscript. We have modified the manuscript accordingly, and the detailed corrections are listed below point by point.

GENERAL COMMENT:

Adekoya et al., 2018 presents observations of ionospheric impacts of the 21 August 2017 Total Solar Eclipse using measurements from a network of ionosondes across the United States. The authors then relate these observations back to theory by fitting the observations to a Chapman type ionosphere. This paper has the potential for being a good contribution to the literature by relating observations during a highly-publicized eclipse event to a well known ionospheric model. However, I believe that the manuscript requires substantial revision before it can be published in *Annales Geophysicae*.

Major comments:

Comment 1

- Section 2 (Data source, methodology, and path of the eclipse) would benefit greatly by being expanded and broken into sections. Suggestions include:
 - a. Add a figure that shows the path of the eclipse, the percentage of maximum obscuration, and location of the ionosondes. This is especially important as you cannot guarantee that the websites you list for path information will always exist.

Response to Comment a

- ✓ We have added an orthographic projection map showing the coverage area and the circumstances of the solar eclipse, see figure 1 and line 65 - 66.

- b. Add a figure using actual data from the event showing how you fit the Chapman profile, and identify the parameters derived (H , B_0 , B_1). Add text explaining how this allows you to draw conclusions relating the topside ionosphere to bottomside measurements.

Response to Comment b

- ✓ We have added a profiler (Figure 6) that illustrates the relationship between the bottomside and the topside parameters, using the actual data of the event and the corresponding non-eclipse period, and texts explaining how the Chapman profile can be fitted (see line 92 – 104 and line 281 – 289).

Comment 2

- Figures 1 & 2:
- a. I don't understand why you ordered the ionosondes in the manner that you did. Could you please order them from west (top) to east (bottom)? This is also the order in which the eclipse progressed across the UT.

Response to Comment a

✓ The ionosonde stations have been reordered according to the eclipse progression time.

- b. Instead of using LT as your X-axis, try using time relative to eclipse maximum, with 0 in the center. This way, it will be easy to compare the effect at all stations. To show local time, add another dashed or dotted line to each panel showing the local solar zenith angle. Put the solar zenith angle on the right-hand y-axis.

Response to Comment b

✓ We did use the local time (LT) corresponding to the start (S), maximum contact (M) and last contact (E) of the eclipse, which made it more easy to compare the effect locally. In Table 1, both the universal time (UT) and the local time progression of the event have been provided. The UT and LT difference for each station is also presented. All these will help the reader to easily relate the eclipse effect at each station.

- c. In the caption, add some text guiding the reader of what eclipse signature to look for and why.

Response to Comment c

✓ Text on the expected signature has been added.

Comment 3

- Figure 3
- a. The biggest problem here is that the Point Argello panel is dominantly green, but there are no green values in the colorbar. This absolutely must be fixed. For the colorbar, consider using a symmetric, diverging color map. Say, red-white-blue (like below) with the range -65% to +65%.



Response to Comment a

✓ We really appreciate the reviewer for this wonderful correction. We prudently carried out the correction as suggested and the end result was astonishing and well represented (see Figure 4).

- b. I'd recommend fixing the Y-axis to some symmetrical value (say +/- 25) for all stations for easy comparison.

Response to Comment b

✓ The Y-axis has been fitted, using symmetry interval unit value, because maximum value along Y-axis is not symmetry for all the plots. And if we try to set it above the maximum, it will only show open spaces that will raise some doubting questions in the mind of the readers.

- c. As for figures 1 & 2, I'd recommend plotting the x-axis in hours relative to eclipse maximum.

Response to Comment c

✓ The figures were plotted for the daytime periods (i.e., from sunrise to sunset period). Having understood the contribution of photoionization to the plasma distribution in the ionosphere, solar eclipse presents the consequences of the sudden loss in the photoionization during the daytime. Therefore, it will be advisable to observe the state of the ionosphere before and after the eclipse for better understanding of its problems and morphology. Moreover, it will inform the readers the clear picture of the effect of reduction in photoionization.

- d. Order the panels from west to east (or some other way that makes sense according to what you are trying to show).

Response to Comment c

- ✓ This, we had attended to (see comment 2a)

Comment 4

- There are numerous grammatical errors. Some are minor, but some are major. For example, line 284 does not make sense. It currently reads, "Hence their relationship in describe one another is established."

Response to Comment

- ✓ Careful proofread of the manuscript has been done and all the language and typographical errors were corrected.
- ✓ We have checked and modified the statement accordingly (see line 307 – 308).
- **Minor Comments**
- **1. Line 56: "This," à "Thus,"**
 - ✓ Corrected (see line 55)
- **2. Line 59: "result and discussion were" à "results and discussion are"**
 - ✓ Corrected, now reads results and discussion (line 58).
- **3. Line 83: Kp is unitless (not nT)**
 - ✓ This was a mistake, now corrected (see line 83).
- **4. Line 152: "recombination too" à "recombination, too"**
 - ✓ Corrected, now in line 163
- **5. Line 200: "This imply" à "This implies"**
 - ✓ Corrected, now in line 215

Best regards,

ADEKOYA, B. J.(Ph.D)

For the Authors

RESPONSE TO ANONYMOUS REVIEWER 2 COMMENTS

MS No.: angeo-2018-35

MS Type: Regular paper

Iteration: Minor Revision

MANUSCRIPT TITLE: **Solar Eclipse-Induced perturbations at mid-latitude during the 21 August 2017 event**

Dear Editor,

GENERAL RESPONSE

We thank the reviewer for the useful and supportive corrections/suggestions. We believed that all suggestions made by the reviewers' have been attended to accordingly. Major corrections have been carried out and are highlighted (red colour) in the manuscript. More figures have been added as suggested by another reviewer, this has made the initial figure numbers to be reordered. The table has been edited to highlight the corresponding local time to the universal time of the solar eclipse progression. all additional references quoted in the text had been included in the reference list and highlighted in red colour.

Further, the names of the authors appears only because of their contributions in planing, data analysis and writing the report. Therefore, two more authors who participated largely in the review processes from the first submission to present have been added. The Authors list now reads "*Bolarinwa J. Adekoya, Babatunde O. Adebesin, Victor. U. Chukwuma, Timothy W. David, Stephen O. Ikubanni, Shola J. Adebisi, and Olawale. S. Bolaji*" based on their contributions. The third author was/is my Ph.D supervisor/mentor who have contributed majorly to my academic growth till present. The last author is a senior colleague that rendered his help when we had problem in some key area during the revisions. Not only that, he partook in the general proofreading/editing of the manuscript.

The authors are grateful for the useful comments and suggestions on the structure of the manuscript. This has tremendously improved the standard of the manuscript. We have modified the manuscript accordingly, and the detailed corrections are listed below point by point:

Major concerns:

Comment 1

- For Comment 2 of first version of manuscript, the authors corrected "percentage obscuration" but didn't correct "percentage deviation" in the manuscript.

Response to Comment 1

- ✓ This is an oversight and have now corrected in the edited version

Comment 2

- In Figures 1 and 2, it is clear that NmF2 goes down during eclipse time, but for hmF2, scale height, bottomside, the curves fluctuate sharply, with a lot of spikes, so it is hard to draw a convincing conclusion.

Response to Comment 2

- ✓ We have replotted the figures to clearly show the morphology of the ionospheric characteristics during the eclipse window.

Comment 3

- Line 141-143, the authors said "The ionosphere over Eglin AFB, Boulder, Point Arguello, Millstone Hill and Idaho National Lab, did not show any contrary variation to that observed at Austin during the eclipse event. The decrease and increase in NmF2 and hmF2 after the maximum magnitude was simultaneous." But I don't agree with it. First, I didn't find that NmF2 and hmF2 change simultaneously. Second, I don't think the variations between these stations are consistent. Please analyse these stations one by one. For example, for NmF2, it is really clear that it goes down from S to M and goes up from M to E. However, for hmF2, it is totally different, as shown in the table below.

The variation of hmF2 during eclipse compared to control day
Station from S to M from M to E

Austin Up Down

Eglin AFB Not available Not available

Boulder No apparent trend Down

Point Arguello Up A valley

Millstone Hill No apparent trend Down

Idaho National Lab No apparent trend DownPP46: “However”, should be deleted, and star the sentence simple -
At equatorial and low-latitudes...

Response to Comment 3

- ✓ We appreciate the reviewer for this observation, this has tremendously improved our data analysis. The discrepancies have now been corrected and the figure have been replotted. The figures are more clearer and explained the simultaneity in the ionospheric variations observed at the eclipse window better.

Comment 4

- Line 175-176, the authors said “It was observed from the plots that the minimum decrease in NmF2 amplitude corresponds to increase in H at all stations”
But at least at Austin and Eglin AFB, I didn’t find the conclusion above.
- Line 205-206, the authors said “B1 responded with a decrease at the first contact of the eclipse compared to the control day.”
But at least at Austin, Eglin AFB, Milestone Hill, Idaho National Lab, I didn’t find the conclusion above.
- Line 207-209, the authors said “B0 parameter from the first contact increases and reached the maximum peak few minutes after the maximum obscuration magnitude, which coincided with the minimum decrease in B0.”
But at least at Austin, Eglin AFB, Milestone Hill, I didn’t find the conclusion above.

Response to Comment 4

- ✓ As said earlier, all the figures have been regenerating. Kindly check the highlighted texts in the reviewed manuscript

Comment 5

- In Figure 1, there are no available data during and after eclipse at Eglin AFB. However, in Figure 3, the percentage of deviation at Eglin AFB is complete. How did you get this?

Response to comment 5

- ✓ The data gap in Eglin AFB, Figure 4 (old figure 3) was interpolated by the software used in generating the plot. However, the Eglin AFB plot has been removed from Figure 4 for the benefit of doubt on the description of the ionospheric behavior over the station.

Comment 6

- I have to say, I haven’t yet understood Figure 3. I guess in this figure, DNmF2 is the ratio of the electron density at different height between eclipse day and control day, that is to say, it may be $((Ne)_e - (Ne)_c)/(Ne)_c \times 100$, but the authors said “was defined as the ratio of $((NmF2e - NmF2c)/NmF2c) \times 100$.” So I am really confused by DNmF2. For a certain local time at one station, there are only one NmF2e and one NmF2c.

Response to Comment 6

- ✓ We believed that figure 4 (old figure 3) was used to described the neutral wind flow and thermospheric compositions during solar eclipse (see line 235 – 273). The $\delta NmF2$ is the percentage deviation of the maximum electron density at the F2 layer, while the Ne is the electron density at different altitude of the ionosphere. Whereas, NmF2e and NmF2c are the maximum electron density of the F2 layer during the eclipse and non-eclipse (i.e., control period, which is the average of the respected non-eclipse days). Indeed, for a certain period of local time there is only one NmF2e and NmF2c, for every period of the day, the the NmF2 plot is plotted. However, we have plotted in figure 6, the electron density profile that explain the distribution of the electron at different altitude during solar eclipse and the corresponding non-eclipse period.

Comment 7

- Moreover, in Figure 3, at Point Arguello, the colour scale didn't show the green.

Response to comment 7

- ✓ In Figure 3 (now Figure 4) we have replotted the figure, changing the colour legend and the axis scaling to clearly shows the simultaneity in the colour distribution.

Comment 8

- For Comment 5 of first version of manuscript, the reviewer asked a questions "Line 241-242, the authors said "The only exception ... at Millstone... H versus B0 ..." however, it is clear that R is also low for the two figures of IDAHO."

But this time, in second version of manuscript, Line 262 to 264, the authors said "The only exception where low correlation was observed was at Idaho (0.47) and Millstone (0.37) with respect to the H versus B0 relationship." So the correlation at Idaho (0.52) with respect to H versus hmF2 is not an exception? In fact, in Figure 4, only at Point Arguello and Millstone Hill, the correlation is good enough.

- If the authors are not able to explain height parameters properly, just showing them directly without convincing processing and analysis, I don't think this manuscript is worth being published.

Response to Comment 8

- ✓ All the discrepancies have been corrected. Figure 4 (now Figure 5) has been replotted. More explanations have been provided in the text on the height parameters, which allows to drawn conclusions relating the topside ionosphere to bottomside measurements.

Best regards,

ADEKOYA, B. J.

For the Authors

SOLAR ECLIPSE-INDUCED PERTURBATIONS AT MID-LATITUDE DURING THE 21 AUGUST 2017 EVENT

Bolarinwa J. Adekoya¹, Babatunde O. Adebisin², Victor. U. Chukwuma¹, Timothy W. David¹,
Stephen O. Ikubanni², Shola J. Adebisi², and Olawale. S. Bolaji^{3,4}

¹Department of Physics, Olabisi Onabanjo University, P.M.B. 2002, Ago Iwoye, Nigeria

²Space Weather Group, Department of Physical Sciences, Landmark University, P.M.B 1001, Omu-Aran,
Kwara State, Nigeria

³Department of Physics, University of Lagos, Akoka – Yaba, Lagos, Nigeria

⁴Department of Physics, University of Tasmania, Hobart, Australia

Correspondence to: Bolarinwa J. Adekoya (adekoyabolrinwa@yahoo.com; adekoya.bolarinwa@oouagoiwoye.edu.ng)

Abstract

A study of the response of some ionospheric parameters and their relationship in describing the behaviour of ionospheric mechanisms during the solar eclipse of 21 August 2017 is presented. Mid-latitude stations located along the eclipse path and with data availability on the Global Ionospheric radio Observatory (GIRO) database were selected. The percentage of obscuration at these stations range between 63-100%. Decrease in electron density during the eclipse is attributed to reduction in solar radiation and natural gas heating. The maximum magnitude of the eclipse coincided with $hmF2$ increase and with a lagged maximum decrease in $NmF2$ consistently at the stations investigated. The results revealed that the horizontal neutral wind flow is as a consequence of the changes in the thermospheric and diffusion processes. The unusual increase/decrease in the shape/thickness parameters during the eclipse period relative to the control days points to the perturbation caused by the solar eclipse. The relationship of the bottomside ionosphere and the F2 layer parameters with respect to the scale height are shown in the present work as viable parameters for probing the topside ionosphere during eclipse. Furthermore, this study shows that in addition to traditional ways of analysing the thermospheric composition and neutral wind flow, proper relation of standardized $NmF2$ and $hmF2$ can be conveniently used to describe the mechanisms.

Keywords: solar eclipse; solar radiation; bottomside profile parameters; $NmF2$ and $hmF2$; Topside ionosphere; GIRO database.

1 Introduction

Solar eclipse provides opportunity to study the causes of drastic changes in the atmosphere arising from reduction in solar radiation and plasma flux. The atmosphere responded to these changes by modifying the electrodynamic processes and ionization supply of its species to the nighttime-like characteristics during the daytime. Different physical mechanisms (e.g. neutral wind, thermospheric composition, diffusion process etc.) that explain the distribution of plasma at the different ionospheric layers are well established. However, these mechanisms do compete with themselves in explaining the ionosphere, especially the topside ionosphere (see Gulyaeva, 2011).

At mid-latitudes, the effect of diffusion processes and its relationship with the thermospheric compositions has been extensively studied during episodes of solar eclipse (Muller-Wodarg et al., 1998; Jakowski et al., 2008; Le et al., 2009; Wang et al., 2010; Chuo, 2013). At equatorial and low-latitude regions, the $E \times B$ plasma drift had been used to explain the circumstances of solar eclipse on transport processes (Adeniyi et al., 2007; Adekoya et al., 2015). Recently, attention has been drawn to the study of the topside ionosphere during an eclipse for improved prediction and modelling (Huba and Drob, 2017; Chrniak and Zakharenkova, 2018). Reinisch et al., (2018) compared the modelled and measured studies of electron densities at the altitude range of about 150 - 400 km during the eclipse. They found that at lower altitude (at about 150 km) the modelled and the measured agreed well to the changes in the altitude profile of electron density compared to at higher altitudes. The authors however posited that it would be improved if the model $NmF2$ peak falls more slowly to better match the data. Consequently, the present study investigates the effects of solar eclipse of August 21, 2017 on the constituents of the ionosphere at mid-latitudes using some ionosonde data (bottomside parameters, scale height (H) estimated from the fitted α -Chapman layer) which have not been given much attention in previous works especially in analysing solar eclipse effect. Using these parameters to analyse the circumstances of solar eclipse at the topside ionosphere and its plasma distribution mechanisms make this paper significantly different from previous studies. Thus, we intend to achieve by analysing the ionospheric parameters that controls the distribution of plasma at the topside and bottomside layers of the F2 region. To shed light on these analysis, section 2 highlights the data source, methodology, and path of the eclipse. The results and discussion were presented in section 3, while section 4 presents the summary and concluding remark of the result.

62

63 2 The solar eclipse path and Data source

With regards to the eclipse of 21 August 2017, the totality of the eclipse is visible from within a narrow corridor that traverses the United States of America. However, in the surrounding areas, which include all of mainland United States and Canada, the eclipse was partial. From the footprint of the Moon's shadow as seen from some locations, the eclipse started from around 17:00 UT and ended around 20:00 UT. Figure 1 shows the detail coverage area and circumstances of the solar eclipse. More details of its path can be seen via NASA – Total solar eclipse of 2017 August 21 (<https://eclipse.gsfc.nasa.gov/>). The details on the local circumstances of the eclipse, the time of the first, mid and last contact of the eclipse over the ionosphere of the investigated stations was highlighted in table 1. More details on the total solar eclipse event and its partiality, the circumstances surrounding its progression and its magnitude of obscuration can be obtained through the link http://xjubier.free.fr/en/index_en.html. The path of the eclipse informed the choice of stations. The ionospheric data used for this study for the selected mid-latitude stations were obtained from the Global Ionospheric Radio Observatory (GIRO) networks, <http://giro.uml.edu/> (Reinisch and Galkin 2011) and manually validate. The calculated daily average of summation K_p , A_p and solar flux indices was

obtained from the National Space Science Data Centres (NSSDC's) OMNI database <https://omniweb.gsfc.nasa.gov/>.

3 Methods of data analysis

$NmF2$ values for both the eclipse and control days were obtained from their corresponding critical frequencies ($foF2$) using the expression: $NmF2 = ((foF2)^2 / 80.5) \text{ e/m}^3$. The control day value is the average value of the two days before/after the eclipse day (i.e. 6, 12, 24 and 27). These reference days were chosen such that they have similar geomagnetic, interplanetary and solar properties with the eclipse day. The daily average value of control days and eclipse day interplanetary index (Ap and Kp), and solar flux unit index ($F10.7$) ranges from 8 – 12 nT for Ap , 2 – 3 for Kp index and 75.6 – 89.1 sfu (1 solar flux unit (sfu) = $10^{-22} \text{ Wm}^{-2} \text{ Hz}^{-1}$) for $F10.7$, indicating that geomagnetic and solar activities of these days is unsettled (see Adekoya et al., 2015 for classification of geomagnetic activity). The typical behaviour of the $NmF2$ and $hmF2$ on the eclipse day (i.e. $NmF2e$ and $hmF2e$) was compared with that of the control day ($NmF2c$ and $hmF2c$) to observe the changes brought by the short period of loss of photoionization in the ionosphere. This will measure the direct consequence of the solar radiation disruption (due to the eclipse) on the ionospheric chemical, transport and thermal processes in the F2 layer. The ionized layer depends majorly on three parameters, viz: $NmF2$, $hmF2$, and the plasma scale height (H_m).

The GIRO provides access autoscaled values of ionospheric parameters generated by Automatic Real-Time Ionogram Scaler with True height (ARTIST) algorithm, which is inherent in the UMLCAR-SAO Explorer (Reinisch and Huang 1983; Galkin et al., 2008; Reinisch and Galkin 2011), facilitates the derivation of bottomside profiles. From the UMLCAR-SAO Explorer, the manually scaled ionogram with high accuracy are calculated from the standard true-height inversion program (Reinisch and Huang, 1983; Huang and Reinisch, 1996). The parameters obtained include the critical frequency ($foF2$, Hz), and its height ($hmF2$, km) of the F layer and the shape parameter ($B1$), and the thickness parameter ($B0$). Likewise, the scale height (H_m) of the F2 layer is obtained from the bottomside. It is estimated from the fitted α -Chapman function with a variable scale height, $H(h)$, to the measured bottomside profile $N(h)$, which then determined as the Chapman scale height at $hmF2$ (i.e. $H(hmF2) = H_m$) (Huang and Renisch 2001; Reinisch and Huang 2001; Reinisch et al., 2004). The topside profile is then related to the scale height at the layer, from the bottomside profile, represented with α -Chapman function (Reinisch and Huang, 2001). This is because the Chapman function described the electron density profile, $N(h)$ aptly. Also, H_m provides a linkage between the bottomside ionosphere and the topside profiles of the F region (Liu et al., 2007). Therefore, H_m describes the constituents of the ionospheric plasma, which decreases with increasing altitude.

111 However, Xu et al. (2013) and Gulyaeva (2011) related ionospheric F2 - layer scale height, H to the topside
112 base scale height, H_{sc} , given by $H_{sc} = h_{sc} - h_m F2 \approx 3 \times H_m$. Where h_{sc} is the height at which the electron
113 density of the F2-layer falls by a factor of an exponent, at an upper limit of 400 km altitude (i.e. $NmF2/e$)
114 (see Xu et al., 2013). That is, the region where electron density profile gradient is relatively low. Gulyaeva
115 (2011) showed theoretically that H_{sc} increase over H_m by a factor of approximately three (3) and is a
116 consequence of the $Ne/NmF2$ ratio (Ne – plasma density), which corresponds to H_m in the Chapman layer.
117 At altitudes very close to $h_m F2$, the ratio equals 0.832, while it is 0.368 at altitudes beyond the $h_m F2$.
118 Therefore, we adopted the definition of Gulyaeva (2011) for the topside base scale height as the region of
119 the ionosphere between the F2-peak and 400 km altitude. Summarily, the topside based scale height
120 ionosphere here is defined as the region between the F2 peak and h_{sc} or $3H_m$. It is thus evident that H is a
121 key and essential parameter in the continuity equation for deriving the production rate at different
122 altitudes, a pointer to the F2 topside electron profiler, as well as a good parameter for evaluating the
123 transport term (Yonezawa, 1966; Huang and Reinisch, 2001; Reinisch and Huang, 2001; Belehaki et al.,
124 2006; Reinisch et al., 2004). Consequently, the parameter H_m can be used as a proxy for observation
125 relating to the topmost side electron density profile. Furthermore, the division of the topsides and the
126 bottomside ionosphere may be related to the difference in the effective physical mechanisms in the
127 regions. Hence, the bottomside parameters $B1$ and $B0$ of the ionosphere, as presented in this work, helped
128 in examining the perturbation of solar eclipse in the bottomside ionospheric F2 layer.

129

130 **4 Results and Discussion**

131 This section presents the temporal evolution of the maximum electron density ($NmF2$), and its
132 corresponding height ($hmF2$) over the ionosphere at the selected mid-latitude stations along the path of
133 solar eclipse of 21 August 2017. The control day variation relative to the eclipse day is also presented.
134 Figure 2 presents the variation of maximum electron density and the corresponding peak height, during
135 both the eclipse and control days. Figure 3 depicts the variation of scale height and the bottomside
136 parameters ($B0$ and $B1$) due to the eclipse by superposing plots for both the eclipse and control days.
137 Analysis of these parameters during an eclipse event may help in the modelling of the ionospheric profiles
138 (the topsides and bottomside electron density distribution profile) during the short nighttime-like period of
139 the day. Figure 2a presents the $NmF2$ and $hmF2$ variations during the eclipse event and the control day
140 over the Idaho National Lab; having an obscuration magnitude of 100% around the daytime period. The
141 effect of the disruption of solar radiation was evident as the $NmF2$ started decreasing at the first contact of
142 the eclipse compared to an incessant increase on the control day in Fig. 2ai. The start time or first contact
143 (08:43:31 LT), the maximum magnitude period (10:01:53 LT) and the end time or the last contact (11:25:46
144 LT) of the eclipse are marked with the vertical lines S, M and E respectively. The decrement in $NmF2$ during
145 the eclipse phase was due to reduction in the ionization. This reduction caused changes in the

146 photochemical and transport process of the atmosphere during the daytime, thus exhibiting nighttime
147 characteristics. It should be noted that the maximum decrease in $NmF2$ did not coincide with the maximum
148 magnitude of the eclipse obscuration, rather with a time lag of few minutes, i.e., 1030 LT. This lag period
149 fell within the relaxation period over Idaho ionosphere, with $NmF2$ and $hmF2$ simultaneously attaining their
150 peak magnitudes of 1.67 e/m^3 and $\sim 239 \text{ km}$. Hence, the ionosphere returned to its pre-eclipse state.
151 Contrary to the decrease in the $NmF2$ amplitude at the recovery phase of the eclipse, the $hmF2$ increases,
152 attained 239 km peak around 1030 LT and then decreases depicting the eclipse caused morphology.

153
154 The ionosphere over Boulder, Eglin AFB, Austin, Millstone Hill and Point Arguello did not show any contrary
155 variation to that observed over Idaho during the eclipse event. The decrease and increase in $NmF2$ and
156 $hmF2$ after the maximum magnitude are simultaneous. The only exception was that the local time at which
157 each station observed the effects were different. Their obscuration percentage ranged from 62.5 – 93.37%.
158 This did not cause any significant change in the way they responded to the reduction in solar heating. The
159 ionosphere over Boulder experienced the totality of the eclipse with 93.37 % magnitude, which is next to
160 Idaho (100%) in obscuration, the $hmF2$ was observed to increase few minutes after the maximum
161 magnitude of the obscuration. This behaviour is typical for other stations at the eclipse window, but the
162 time of $NmF2$ minimum decrease did not always coincides with the $hmF2$ enhancement after the maximum
163 obscuration. These observations posit that the minimum rate of electron production does not necessarily
164 translate to the peak electron density of the molecular gases formed. This is because the electron
165 concentration depends on the loss rate by dissociative recombination, too.

166
167 At mid-latitudes, the ionospheric F2 plasma distribution is controlled by diffusion processes (Rishbeth
168 1968). There are two basic mechanisms that define the diffusion process during an eclipse: First is the
169 coolness brought by the partial removal of photoionization (Müller-Wodarg et al., 1998), which is believed
170 to instigates the downward diffusion process, and the atmospheric expansion due to the gradual increase
171 in the temperature after the totality. The downward diffusion process was related to the increase in the
172 molecular gas (N_2) concentration during the cooling process. However, the aftermath of the coolness was
173 related to the upward diffusion process. These mechanisms were proxy to the electron density distribution
174 during the eclipse window. Our analysis suggests that the observed decrease in $NmF2$ is due to the
175 downward diffusion flux of the plasma while the increase that followed is by upward diffusion (e.g. Le et al.,
176 2009; Adekoya and Chukwuma 2016). Several works on eclipse (Müller-Wodarg et al., 1998; Grigorenko et
177 al., 2008; Adekoya and Chukwuma 2016; Hoque et al., 2016) have shown that it was not just the electron
178 density that is being affected during an eclipse window, but the thermospheric wind as well, since the
179 thermospheric wind emanating from the ratio of gas species is related to the variation in electron density.
180 It has been observed that the increase in the mean molecular gas of thermospheric composition decreases

181 the electron density and vice versa. Le et al. (2010) related the trough of electron density distribution
182 during the eclipse phases to the contraction/compression and expansion of the atmosphere brought by the
183 decrease and increase in temperature. Chukwuma and Adekoya (2016) attributed the decrease in the
184 electron temperature to the downward vertical transport process and the decrease in the cooling process
185 to the upward vertical transport process.

186

187 Figure 3 describes the variation of H_m , $B1$ and $B0$ in three columns respectively for all the stations. Looking
188 at the H_m plots, one can see that there was a define morphological description of H_m at the eclipse window.
189 From the first contact of the eclipse, there was an incessant increase in peak variation that maximized some
190 minutes after the maximum contact of the eclipse, i.e., about 15 – 45 mins later. Following the peak
191 magnitude of after the maximum contact of the eclipse, the H_m sharply decreases, reaching the minimum
192 peak before its rather increase throughout the remaining period of the eclipse second phase. It was further
193 observed that the minimum decrease in $NmF2$ amplitude corresponds to increase in H_m at all stations;
194 implying the upward lifting of the topside electron to the region of higher altitude at the eclipse window.
195 Hence, the scale height variation highlights the decrease in electron production and the vertical distance
196 through which the pressure gradient falls at the topside during the eclipse activity. The observation
197 illustrates the mutual relationship between the $NmF2$ and H_m , which may aid in extrapolating the topside
198 ionospheric profile (Gulyaeva, 2011). In essence, scale height changes observed during the eclipse window
199 can be used to explain the pressure gradient, electron density distribution and transport processes. In this
200 sense, the diffusion coefficients are expressed as ratio of determinants (determinant here refers to the
201 concentration of species ([O] and [N₂]), with the size of the determinants depending upon both the number
202 of species in the gas mixture and the level of approximation. Therefore, the increase (decrease) in the scale
203 height can be used as a proxy for downward (upward) diffusion process at the topside ionosphere.
204 Consequently, the thermospheric wind, which causes plasma distribution in the topside ionosphere, is
205 induced by solar radiation. Moreover, the significant changes observed in the scale height variation during
206 the eclipse window also indicated that transport processes are affected as they are temperature
207 dependent. Therefore, changes in the thermospheric compositions due to the solar eclipse at the topside
208 layer will affect the density profiles of the ionosphere (Müller-Wodarg et al., 1998).

209

210 It is noteworthy that the increase (decrease) in the scale height decreases (increases) the electron density
211 during the eclipse window. The sensitivity of electron density to temperature at the topside directly affects
212 the electron density profile (e.g. Wang et al., 2010); as cooling due to decrease in temperature results in
213 decrease in the electron density via reduced ionization. This indicates that the decrease (increase) in
214 electron temperature at the topside ionosphere causes the increase (decrease) in the scale height, which is
215 related to the diffusion and transport processes and subsequently affect the pressure gradient of the

216 plasma. From plots of H_m (fig. 3) and $NmF2$ (fig. 2), it was observed that the minimum decrease in $NmF2$
217 corresponded with peak increase in scale height. This implies that the topside ionosphere is more sensitive
218 (than the bottomside) to any changes in the solar radiation. Thus, the pressure gradients can be analysed in
219 terms of either the scale height or electron density during solar eclipse.

220

221 From column 2 and 3 of Figure 3, we observed that the measured shape ($B1$) and thickness ($B0$) parameters
222 of the ionosphere over these stations exhibit significant variations during the eclipse event. $B1$ responded
223 with a decrease at the first contact of the eclipse compared to the control day. This decrease was gradual
224 throughout the eclipse window and followed the variation of solar ionizing radiation. However, $B0$ variation
225 differs to that of the $B1$ observation. The $B0$ increases from the first contact and reached the maximum
226 peak few minutes after the maximum obscuration magnitude, which coincided with the minimum decrease
227 in $B0$. Generally, the pattern of the day to day variation of the bottomside parameters was the average
228 morphology, but the increase in the $B0$ and the decrease in the $B1$ parameters during the eclipse period
229 compared to the control day was a notable one and can be related to the perturbation caused by the solar
230 eclipse. During the eclipse, the solar radiation was lost; trapped atomic ions O^+ was converted into
231 molecular ion (NO^+ and O_2^+) by charge transfer, owing to the sufficient concentration of molecular gasses
232 (N_2 and O_2) (Rishbeth, 1988). The height of the ionospheric slab indeed increased with reduced width,
233 which is attributable to compression due to loss of solar heating.

234

235 The behaviour of the ionosphere can be explained during solar eclipse with any of the components that
236 constitute the topside and the bottomside ionosphere and can be looked at, from the angle of the
237 percentage of concentration of the components. In this regard, the deviation percentage of $NmF2$ ($\delta NmF2$)
238 and $hmF2$ ($\delta hmF2$) during the eclipse day away from the control day were plotted in Figure 4. This is done
239 to describe the contribution of the thermospheric wind and compositions. Although observing the variation
240 of $NmF2$ and $hmF2$ alone can be used for observing the changes in the behaviour of the thermospheric
241 compositions and wind flow, if properly analysed, but it is more convenient to describe these mechanisms
242 by standardizing the original variables used during the event. The normalization effort (with the use of
243 $\delta NmF2$ and $\delta hmF2$) presents the original variation of $NmF2$ and $hmF2$ onto directions which maximize the
244 variance. Consequently, the result can be used for analyses of any mechanisms that drive the ionospheric
245 plasma, if properly related.

246

247 The deviation percentage in Figure 4 was defined as the ratio of $((NmF2e - NmF2c)/NmF2c) \times 100$. The
248 same relation is defined for the $hmF2$ parameter. As earlier pointed out, during eclipse period, neutral
249 composition becomes the dominant chemical process arising from diffusion activities. The increase in the
250 neutral composition leads to the increase in the molecular gas concentration and compete with diffusion

251 process. Hence the deviation percentage discusses the neutral composition changes and delineate how
252 these changes may affect the electron densities as well as its profiles in the atmosphere during the eclipse.
253 The respective maximum and minimum peak response of the deviation percentage is attributed to the
254 enhancement and depletion of $\delta NmF2$. One can see from the plots, the deviation percentage started
255 increasing at the first contact of the eclipse (the first dashed vertical line) and reached the maximum,
256 appearing few minutes after the maximum magnitude of the eclipse (the second dashed vertical line). This
257 behaviour is similar to the conditions of the neutral compositions during the eclipse event reported by
258 Muller-Wodarg et al. (1998).

259

260 Another important process observed in this study is the neutral wind flow effect. To identify the direction
261 of the wind, the $\delta NmF2$ colour legend in the contour plots was used in Figure 4. The negative values
262 represent a westward wind contribution and the positive values is for the eastward wind. Looking at the
263 marked eclipse region in the figure, it was revealed that the $\delta NmF2$ started decreasing from the first
264 contact of the eclipse, maximized few minutes after the maximum contact mark and, thereafter decreases.
265 It has been established that at daytime, the peak height of the plasma will be reduced due to loss in
266 recombination. At nighttime, equatorward neutral wind drives the F2-layer plasma to higher altitudes
267 where recombination rate is slower. The ionospheric processes during solar eclipse is said to represent a
268 partial nighttime/sunset ionospheric process (Adekoya et al., 2015; Adekoya and Chukwuma, 2016). Thus,
269 the F2 plasma behaviour at the eclipse window is induced by the equatorward neutral wind flow. The
270 neutral wind acts jointly with the plasma flows from the topside ionosphere, resulting in F2 region plasma
271 density variation. Therefore, the westward/eastward neutral wind flow is related to the
272 depletion/enhancement in the deviation, which was clearly shown in the marked eclipse region of the
273 figure. The plots in Figure 3 had established the ionospheric dynamics of diffusion processes, neutral
274 compositions and the flow of neutral wind caused by the eclipse perturbation, which can invariably reduce
275 the effectiveness and reliability of radio wave propagation.

276

277 Relative to the mutual relationship between the topside and bottomside ionosphere, we considered the
278 linear correlation coefficient (R) of H_m versus $hmF2$ and H versus BO during the eclipse window. In Fig. 5., R
279 ranges from (0.80 - 0.90) for $H_m/hmF2$ relationship, and 0.57-0.89 for the H_m/BO connection. This good
280 linear agreement revealed the dependence of $hmF2$ and BO on the scale height. Apart from revealing the
281 dependence between the parameters, the relationship may also provide a convenient way for modelling
282 the topside profile from the knowledge of the bottomside parameter, BO , during the eclipse period.
283 Further, fig. 6 illustrates the relationship between the bottomside (continuous line) and the topside
284 (dashed line) ionosphere over Idaho National Lab during solar eclipse compared to the non-eclipse period.
285 On the left side was the ionospheric profile during the first contact of the eclipse, the middle and right-side

profiles are during the maximum contact and last contact of the eclipse respectively. The black curve represents the profile for the eclipse day (August 21) and the red curve is for the one of the selected reference days, August 27. It is clear from the plots that the ionospheric profiles vary with the solar ionizing radiation at the eclipse window and shows the suitability of using the bottomside F-region for probing the topside ionosphere. This behaviour was typical for the ionospheric profiles from other stations along the path of the eclipse. Also, the strong correlation between $hmF2$ and H_m indicates that there may be some interrelated physical mechanisms controlling the behaviour of the plasma at the topside ionosphere during solar eclipse. That is, $hmF2$ is strongly depends on neutral wind flow and explain the state of thermospheric compositions (e. g. Liu et al., 2006; Fisher et al., 2015). Since all these parameters competes during the eclipse, one can argue that with the accessibility of one, in place of the other (as a consequence of their relationship), the prediction and modelling of the ionosphere can be conveniently achieved.

297

298 **5 Conclusions**

299 This paper presents the induced perturbation of solar eclipse of 21 August 2017 on the ionospheric F
300 parameters and how they describe the mechanisms of the ionosphere at mid-latitude. The perturbation
301 effects and dynamics during a solar eclipse episode using ionospheric F2 parameters ($NmF2$ and $hmF2$), the
302 bottomside profile thickness ($B0$) and shape ($B1$) parameters of electron density and the plasma scale
303 height (H_m), which are not often used for eclipse study, were investigated. These parameters represent the
304 state of the F-region ionosphere. The changes observed during the eclipse phase is related to the reduction
305 in solar radiation and natural gas heating. The $NmF2$ minimum was attained around 30 - 45 minutes after
306 the totality of the eclipse when it decreases to about 65% of its control day. This decrease in $NmF2$ was
307 uplifted to the higher altitude where recombinational rate is reduce compared to the non-eclipse day. The
308 thickness and shape parameters which are often limited to the bottomside F-region were seen as viable
309 parameters for probing the topside ionosphere, relative to the scale height during the eclipse. Therefore,
310 their relationship in describing one another is established. The implication is that eclipse-caused
311 perturbation could have been better explained using some ionosonde parameters. The changes in the
312 neutral wind flow, thermospheric compositions and diffusion processes found their explanation in the
313 behaviour of the F region plasma during eclipse. In addition, it can be concluded that the behaviour of
314 $\delta NmF2$ and $\delta hmF2$ during eclipse can be conveniently used to describe the mechanisms of thermospheric
315 composition and wind flow.

316

317 **Acknowledgements**

318 We acknowledge use of global ionospheric Radio Observatory data provided by ULMCAR
319 (<http://ulcar.uml.edu/DIDBase/>) and the World Data Center for Geomagnetism, Kyoto
320 (<http://wdc.kugi.kyoto-u.ac.jp/index.html>) for geomagnetic activity data. We thank the management team
321 of the national Aeronautics and Space Administration (NASA) service (<http://eclipse.gsfc.nasa.gov>) and
322 http://xjubier.free.fr/en/site_pages/SolarEclipseCalc_Diagram.html for progression and eclipse local

323 circumstances information. The authors thank Professor Ljiljana R, Cander and the **anonymous reviewers**
324 for their constructive corrections and suggestions that tremendously improved the structure and quality of
325 the paper.

326 **References**

327 Adeniyi, J. O., Radicella, S. M., Adimula, I. A., Willoughby, A. A., Oladipo, O. A., and Olawepo, O.: Signature
328 of the 29 March 2006 eclipse on the ionosphere over an equatorial station, *J. Geophys. Res.*, 112 (A6),
329 A06314. <http://dx.doi.org/10.1029/2006JA012197>, 2007.

330
331 Adekoya, B. J., Chukwuma, V. U., and Reinisch, B. W.: Ionospheric vertical plasma drift and electron density
332 response during total solar eclipses at equatorial/low latitude, *J. Geophys. Res.*, 120, 8066-8084.
333 doi:10.1002/2015JA021557, 2015.

334
335 Adekoya, B. J., and Chukwuma, V. U.: Ionospheric F2 layer responses to total solar eclipses at low- and mid-
336 latitude, *J. Atmos. Sol. Terr. Phys.*, 138-139, 136-160. <http://dx.doi.org/10.1016/j.jastp.2016.01.006>, 2016.

337
338 Belehaki, A., Marinov, P., Kutiev, I., Jakowski, N., and Stankov, S.: Comparison of the topside ionosphere
339 scale height determined by topside sounders model and bottomside digisonde profiles, *Adv. Space Res.*,
340 <http://dx.doi.org/10.1016/j.asr.2005.09.015>, 2006.

341
342 Cherniak, I., and Zakharenkova, I.: Ionospheric Total Electron Content response to the great American solar
343 eclipse of 21 August 2017, *Geophys. Res. Lett.*, <http://dx.doi.org/10.1002/2017GL075989>, 2018.

344
345 Chukwuma, V. U., and Adekoya, B. J.: The effects of March 20, 2015 solar eclipse on the F2 layer in the mid-
346 latitude, *Advances in Space Research*, 58, 1720-1731. <http://dx.doi.org/10.1016/j.asr.2016.06.038>, 2016.

347
348 Chuo, Y. J.: Ionospheric effects on the F region during the sunrise for the annular solar eclipse over Taiwan
349 on 21 May 2012, *Ann. Geophys.*, 31, 1891-1898. doi:10.5194/angeo-31-1891-2013, 2013

350
351 Fisher, D. J., Makela, J. J., Meriwether, J. W., Buriti, R. A., Benkhaldoun, Z., Kaab, M., and Lagheryeb, A.:
352 Climatologies of nighttime thermospheric winds and temperatures from Fabry-Perot interferometer
353 measurements: From solar minimum to solar maximum, *J. Geophys. Res.*, 120, 6679-6693,
354 doi:10.1002/2015JA021170, 2015.

355
356 **Galkin, Ivan A. Khmyrov, Grigori M., Reinisch, Bodo W. and McElroy, Jonathan: The SAOXML 5: New Format**
357 **for Ionogram-Derived Data, AIP Conference Proceedings, 974, 160. <http://dx.doi.org/10.1063/1.2885025>,**
358 **2008.**

359
360 Grigorenko, E. I., Lyashenko, M. V., and Chernogor, L. F.: Effects of the solar eclipse of March 29, 2006, in
361 the ionosphere and atmosphere, *Geomagnetism and Aeronomy*, 48 (3), 337-351,
362 <http://dx.doi.org/10.1134/S0016793208030092>, 2008.

363
364 Gulyaeva T. L.: Storm time behaviour of topside scale height inferred from the ionosphere-plasmasphere
365 model driven by the F2 layer peak and GPS-TEC observation, *Adv. Space Res.*, 47, 913-920.
366 doi:10.1016/j.asr.2010.10.025, 2011.

367
368 Hoque, M. M., Wenze, I. D., Jakowski, N., Gerzen, T., Berdermann, J., Wilken, V., Kriegel, M., Sato, H.,
369 Borries, C., and Minkwitz, D.: Ionospheric response over Europe during the solar eclipse of March 20, 2015,
370 *J. Space Weather Space Clim.*, 6 (A36). doi: 10.1051/swsc/2016032, 2016.

371
372 Huba, J. D., and Drob, D.: SAMI3 prediction of the impact of the 21 August 2017 total solar eclipse on the
373 ionosphere/plasmasphere system, *Geophys. Res. Lett.*, 44, 5928-5935.
374 <http://dx.doi.org/10.1002/2017GL073549>, 2017.

375

376 Huang, X. and B. W. Reinisch, B. W.: Vertical electron density profiles from the digisonde network, *Adv.*
377 *space Res.* 18 (6), (6)121 - (6)129, 1996
378
379 Huang, X. and B. W. Reinisch, B. W.: Vertical electron content from ionograms in real time, *Radio Sci.*, 36
380 (2), 335 – 342, 2001.
381
382 Jakowski, N., Stankov, S. M., Wilken, V., Borries, C., Altadill, D., Chum, J., Buresova, D., Boska, J., Sauli, P.,
383 Hruska, F. and Cander, Lj. R.: Ionospheric behaviour over Europe during the solar eclipse of 3 October 2005,
384 *J. Atmos. Sol. Terr. Phys.*, 70, 836-853. <http://dx.doi.org/10.1016/j.jastp.2007.02.016>, 2008.
385
386 Le, H., Liu, L., Yue, X., Wan, W., and Ning, B.: Latitudinal dependence of the ionospheric response to solar
387 eclipse, *J. Geophys. Res.*, 114, A07308. <http://dx.doi.org/10.1029/2009JA014072> , 2009.
388
389 Le, H. Le, Liu, Libo, Ding, Feng, Ren, Zhipeng, Chen, Yiding, Wan, Weixing, Ning, Baiqi, Guirong, Xu, Wang,
390 Min, Li, Guozhu, Xiong, Bo, Lianhuan, Hu: Observations and modeling of the ionospheric behaviors over the
391 east Asia zone during the 22 July 2009 solar eclipse. *J. Geophys. Res.*, 115, A10313.
392 <http://dx.doi.org/10.1029/2010JA015609>, 2010.
393
394 Liu, L., Wan, W., and Ning B.: A study of the ionogram derived effective scale height around the ionospheric
395 *hmF2*, *Ann. Geophys.*, 24 (3), 851-860. www.ann-geophys.net/24/851/2006/ , 2006.
396
397 Liu, L., Le, H., Wan, W., Sulzer, M. P., Lei, J., and Zhang, M. -L.: An analysis of the scale heights in the lower
398 topside ionosphere based on the Arecibo incoherent scatter radar measurements, *J. Geophys. Res.*, 112,
399 A06307, <http://dx.doi.org/10.1029/2007JA012250>, 2007.
400
401 Müller-Wodarg, I. C. F., Aylward, A. D., and Lockwood, M.: Effects of a Mid-Latitude Solar Eclipse on the
402 Thermosphere and Ionosphere - A Modelling Study, *Geophys. Res. Lett.*, 25(20), 3787-3790, 1998.
403
404 Reinisch, B. W., Dandenault, P. B., Galkin, I. A., Hamel, R., and Richards R. P.: Investigation of the electron
405 density variation during the August 21, 2017 Solar Eclipse, *Geophys. Res. Lett.*, doi:
406 10.1002/2017GL076572, 2018.
407
408 Reinisch, B. W. and Galkin, I. A.: Global Ionosphere Radio Observatory (GIRO), *Earth Planets Space*, 63 (4),
409 377-381. <https://doi.org/10.5047/eps.2011.03.001>, 2011.
410
411 Reinisch, B. W., Huang, X., Belehaki, A., Shi, J., Zhang, M., and Ilma, R.: Modeling the IRI topside profile
412 using scale heights from ground-based ionosonde measurements, *Adv. Space Res.*, 34 (9), 2026-2031.
413 <https://doi.org/10.1016/j.asr.2004.06.012>, 2004.
414
415 Reinisch, B. W., and Huang, X.: Deducing topside profiles and total electron content from bottomside
416 ionograms, *Adv. Space Res.*, 27 (1), 23-30. [https://doi.org/10.1016/S0273-1177\(00\)00136-8](https://doi.org/10.1016/S0273-1177(00)00136-8), 2001.
417
418 Reinisch, B. W., and Huang, X.: Automatic calculation of electron density profiles from digital ionograms 3.
419 Processing of bottomside ionograms, *Radio Science*, 18 (3) 477 – 492, 1983.
420
421 Rishbeth, H.: Solar eclipses and ionospheric theory. *Space Science Review*, 8 (4), 543-554.
422 <https://doi.org/10.1007/BF00175006>, 1968.
423
424 Rishbeth, H.: Basic physics of the ionosphere: A tutorial review, *Journal of Institute of The Electronics and*
425 *Radio Engineers*, 58 (6S), S207-S223. doi:10.1049/jiere.1988.0060, 1988.
426

427 Xu, T. L., Jin, H. L., Xu, X., Guo, P. Wang, Y. B., Ping, J. S.: Statistical analysis of the ionospheric topside scale
428 height based on COSMIC RO measurements, J. Atmos. Sol. Terr. Phys., 104, 29 – 38.
429 <http://dx.doi.org/10.1016/j.jastp.2013.07.012> , 2013.
430
431 Wang, X., Berthelier, J. J., and Lebreton, J. P.: Ionosphere variations at 700 km altitude observed by the
432 DEMETER satellite during the 29 March 2006 solar eclipse, J. Geophys. Res., 115, A11312.
433 <http://dx.doi.org/10.1029/2010JA015497> , 2010.
434
435 Yonezawa, T.: Theory of formation of the ionosphere, Space Science Review, 5 (1), 3-56.
436 <https://doi.org/10.1007/BF00179214>, 1966
437
438
439
440
441
442
443
444
445
446
447
448
449
450
451
452
453
454
455
456
457
458
459
460
461
462
463
464
465
466
467
468
469
470
471
472
473

474
475
476
477
478
479
480
481
482
483
484
485
486
487
488
489
490
491
492
493
494
495
496
497
498
499
500
501
502
503
504
505
506
507
508
509
510
511
512
513
514
515
516
517
518

Table Caption

Table 1: List of ionosonde station, geographic coordinate, eclipse progression time and percentage of maximum obscuration.

Figure Captions

Figure 1: The orthographic map showing the coverage area and circumstances of the solar eclipse, and the observatory stations of the total solar eclipse event of August 21, 2017 . The thick blue line region of represents the path of the maximum magnitude of the eclipse and the pale blue lines mark the region of where the partial eclipse is experienced, with the magnitude of partiality.

Figure 2: Ionospheric $NmF2$ and $hmF2$ variations during the eclipse day (black continuous line) and the control day (dash blue line). The three vertical lines represents the different phases of the eclipse (S - start time of the initial phase, M - the period of the maximum magnitude of the eclipse, and E - the end time of the recovery phase or the last contact of the eclipse progression). The local time of the respective eclipse contact points for each station are given in table 1.

Figure 3: The local time variation of the ionospheric scale height and the bottomside (BO and $B1$). The other features are the same as in Fig. 1.

Figure 4: Variation of the deviation percentage of $NmF2$ ($\delta NmF2$) and $hmF2$ ($\delta hmF2$) magnitudes for observing the changes in the behaviour of the thermospheric composition and wind flow related to the loss rate during the eclipse phase. The three vertical dashed lines marked the eclipse start time, the time of maximum obscuration and the last contact time of the eclipse (i.e. eclipse phase). Table 1 highlights the local time contact point of the eclipse corresponding the international standard time (IST) eclipse progression. The direction of wind was identify using the $\delta NmF2$ colour legend, the negative values represents the westward wind direction and the positive values is for the eastward wind.

Figure 5: Linear relationship of H versus $hmF2$ and H versus BO during the eclipse of 21 August 2017 progression phase.

Figure 6: Example of the ionospheric profile at the eclipse window of Idaho National Lab showing the bottomside profile (continuous line) and the modelled topside profile shown as a dashed line. The black curve represents the profile for the eclipse day (August 21) and the red curve is for the one of the selected reference days, August 27. On the left side, was the profile during the first contact of the eclipse, the middle and the right profiles are for the maximum contact and the last contact of the eclipse respectively.

519
520
521
522
523
524
525
526
527
528
529
530
531
532
533
534
535
536

537
538
539
540
541

542

543

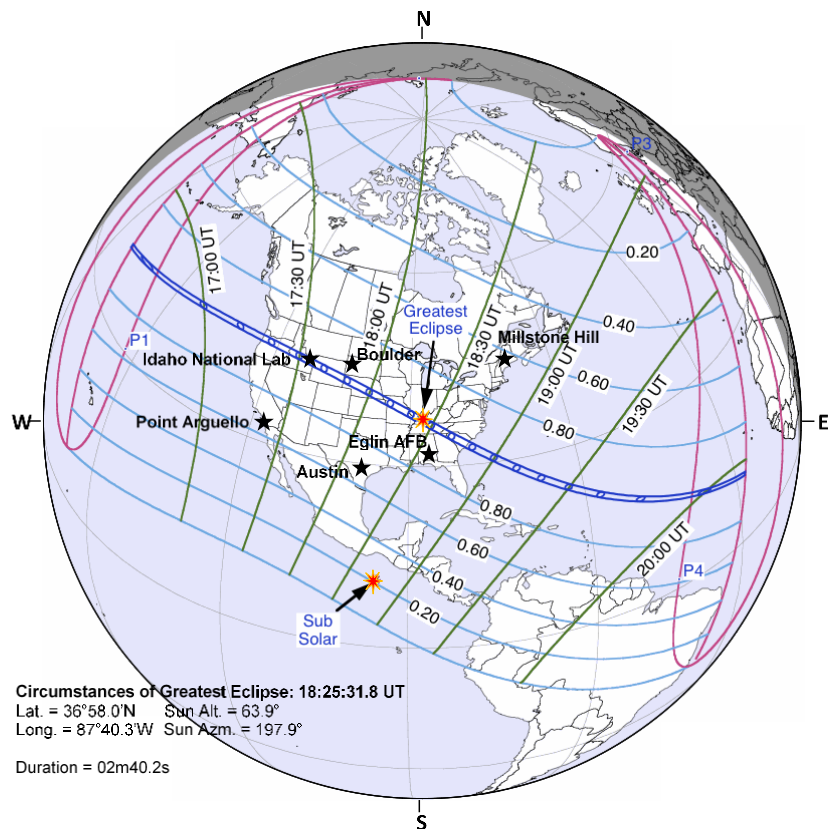
544

545

Table 1: List of ionosonde station, geographic coordinate, eclipse progression time (Universal time/ Local time) and percentage of maximum obscuration.

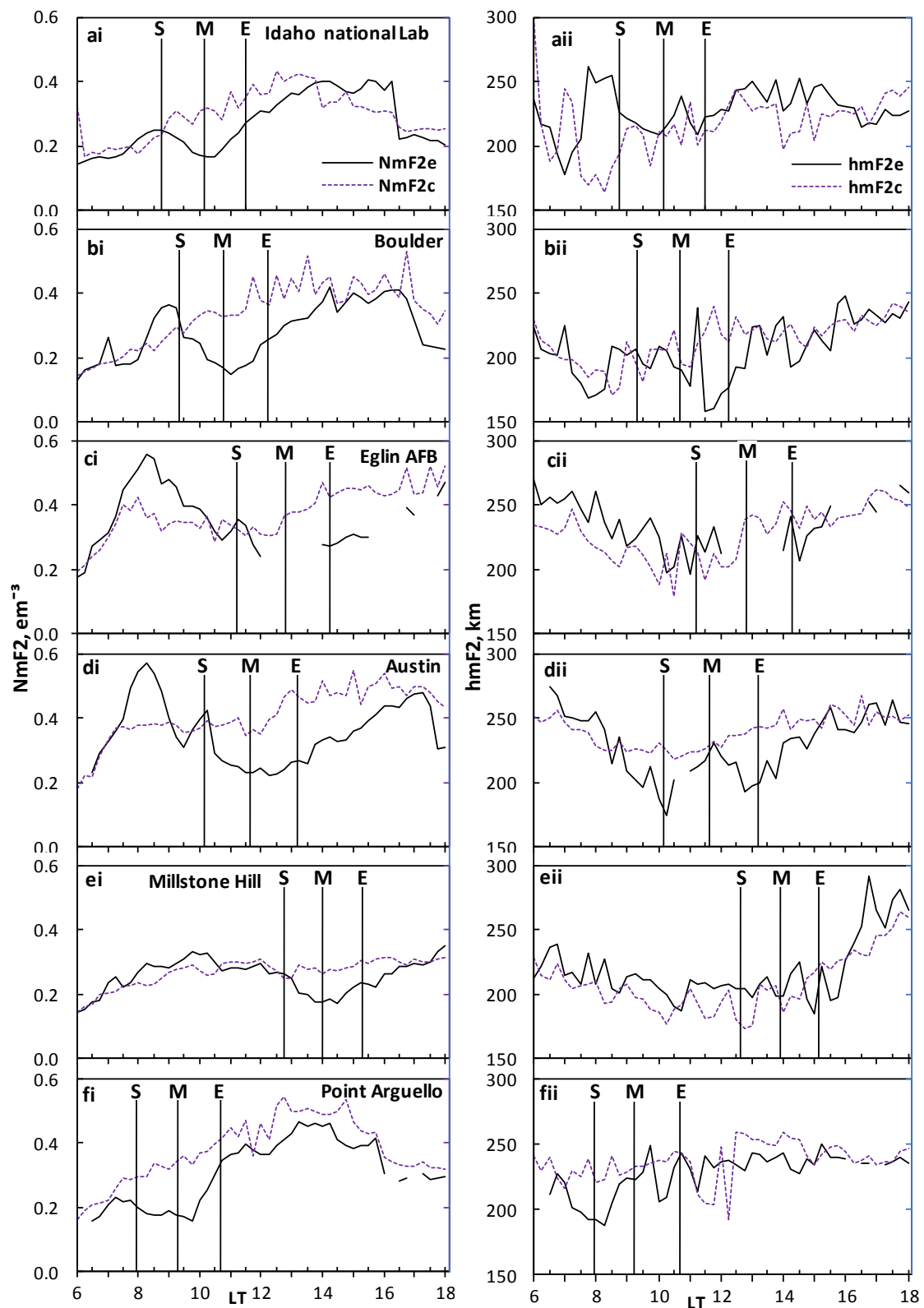
Station	GLat	GLong	Eclipse Start time (UT)/(LT)	Eclipse Max Time (UT)/(LT)	Eclipse End Time (UT)/(LT)	% of max obscuration	UT to LT difference
IDAHO NATIONAL LAB	43.81	247.32	16:14:15/ 08:43:31	17:32:37/ 10:01:53	18:56:30/ 11:25:46	100	16:29:17
BOULDER	40	254.7	16:22:33/ 09:21:21	17:46:10/ 10:44:58	19:13:46/ 12:12:34	93.37	16:58:48
EGLIN AFB	30.5	273.5	17:04:41/ 11:18:29	18:37:08/ 12:50:56	20:03:48/ 14:17:36	83.322	18:13:48
AUSTIN	30.4	262.3	16:40:45/ 10:09:55	18:10:10/ 11:39:20	19:39:35/ 13:08:45	65.93	17:29:10
POINT ARGUELLO	34.8	239.5	16:02:39/ 08:00:15	17:16:55/ 09:14:31	18:39:36/ 10:37:12	64.608	15:57:36
MILLSTONE HILL	42.6	288.5	17:27:28/ 12:41:16	18:45:53/ 13:59:41	19:58:38/ 15:12:26	62.533	19:13:48

546
547
548
549
550



551
552
553
554
555
556
557

Figure 1: The orthographic map showing the coverage area and circumstances of the solar eclipse, and the observatory stations of the total solar eclipse event of August 21, 2017 . The thick blue line region of represents the path of the maximum magnitude of the eclipse and the pale blue lines mark the region of where the partial eclipse is experienced, with the magnitude of partiality.



558

559 **Figure 2:** Ionospheric $NmF2$ and $hmF2$ variations during the eclipse day (black continuous line) and the
560 control day (dash blue line) was presented to delineate effect of solar eclipse of August 21, 2017 on the
561 ionosphere. The three vertical lines represents the different phases of the eclipse (S - start time of the
562 initial phase, M - the period of the maximum magnitude of the eclipse, and E - the end time of the recovery
563 phase or the last contact of the eclipse progression). The local time of the respective eclipse contact points
564 for each station are given in table 1.

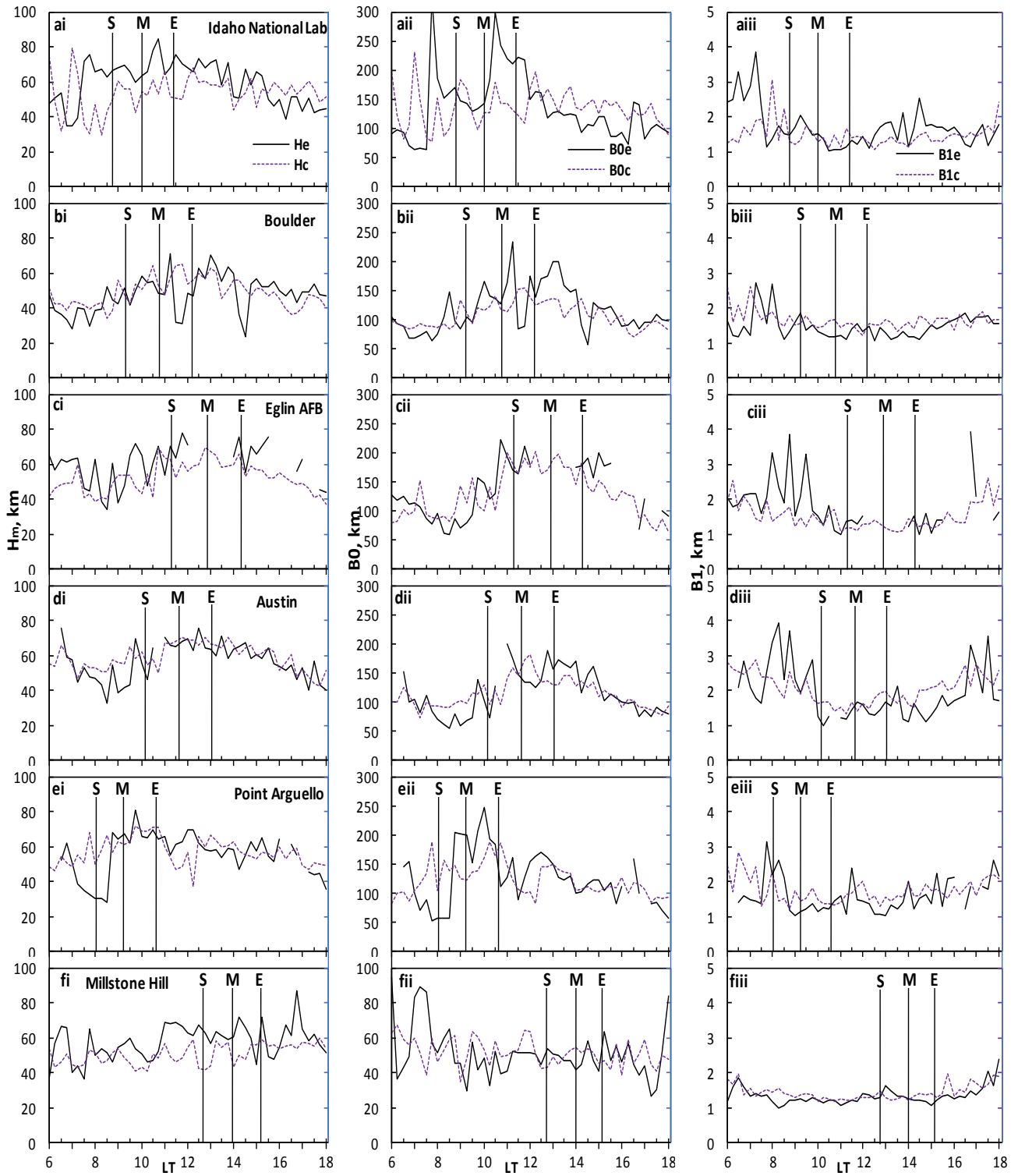
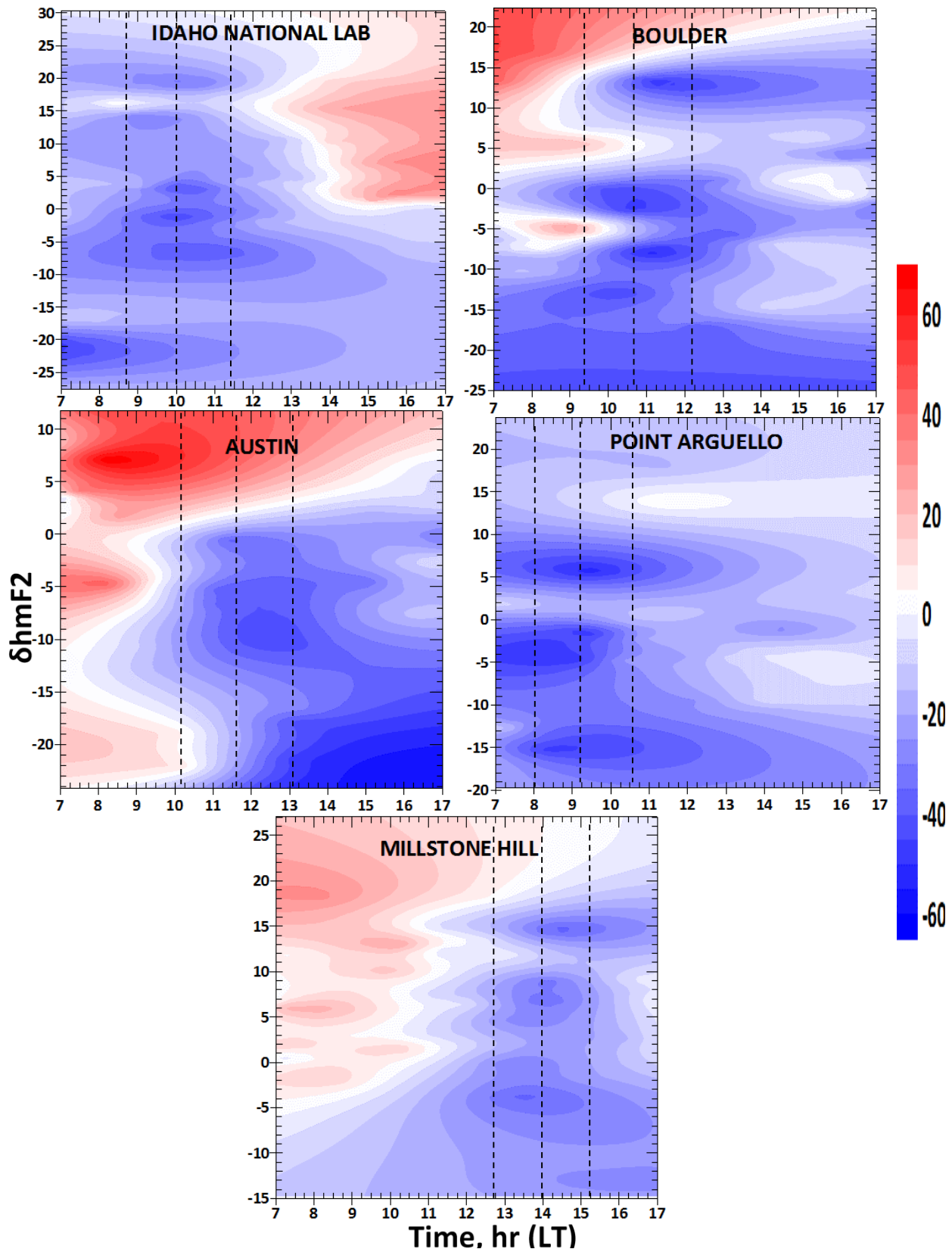


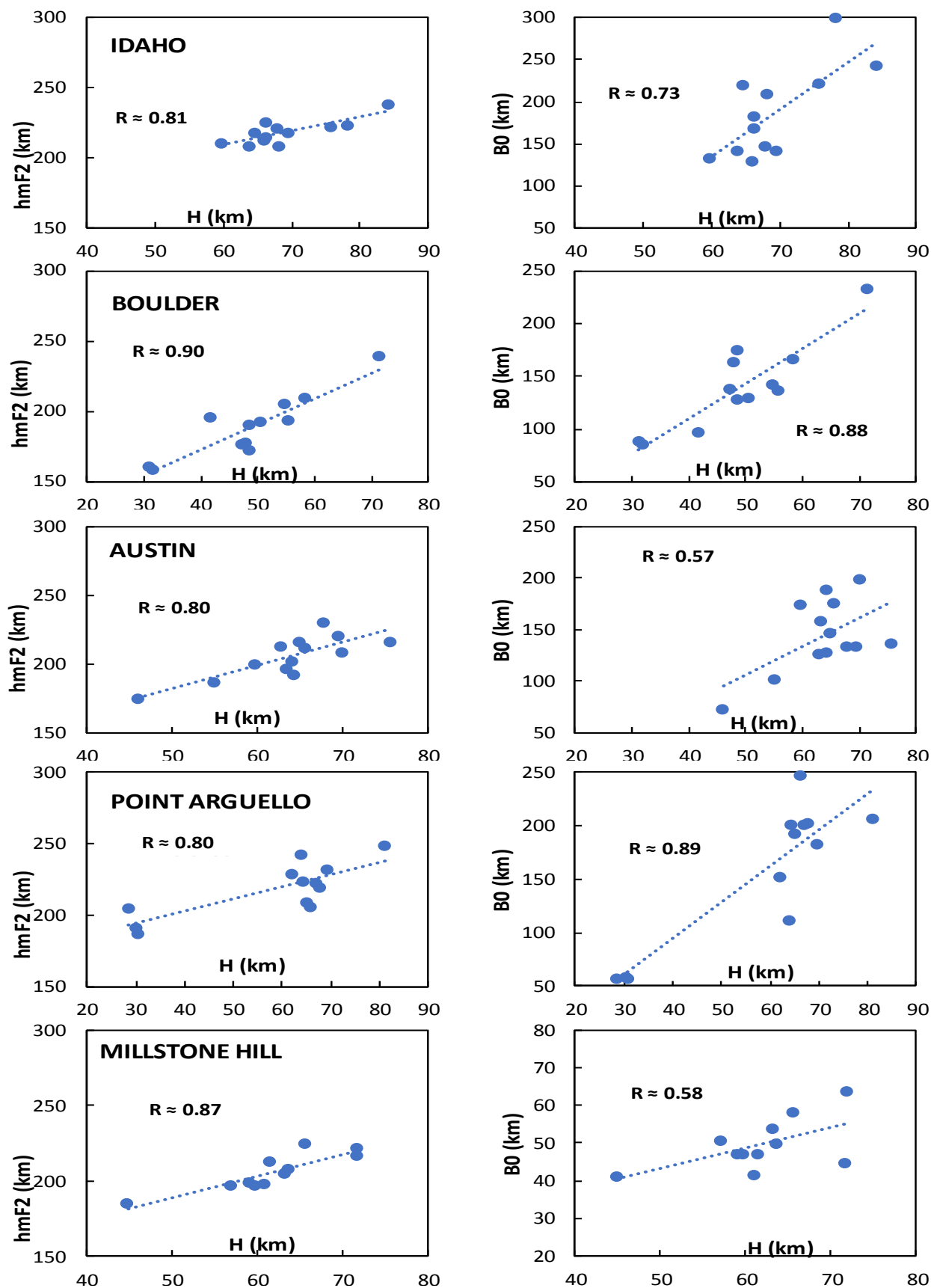
Figure 3: The local time variation of the ionospheric scale height and the bottomside ($B0$ and $B1$). The other features are the same as in Fig. 1.



570

571 **Figure 4:** Variation of the deviation percentage of $NmF2$ ($\delta NmF2$) and $hmF2$ ($\delta hmF2$) magnitudes for
 572 observing the changes in the behaviour of the thermospheric composition and wind flow related to the loss
 573 rate during the eclipse phase. The three vertical dashed lines marked the eclipse start time, the time of
 574 maximum obscuration and the last contact time of the eclipse (i.e. eclipse phase). Table 1 highlights the
 575 local time contact point of the eclipse corresponding the international standard time (IST) eclipse

576 **progression.** The direction of wind was identify using the $\delta NmF2$ colour legend, the negative values
 577 represents the westward wind direction and the positive values is for the eastward wind.



578
 579 **Figure 5:** Linear relationship of H versus $hmF2$ and H versus $B0$ during the eclipse of 21 August 2017
 580 progression phase.

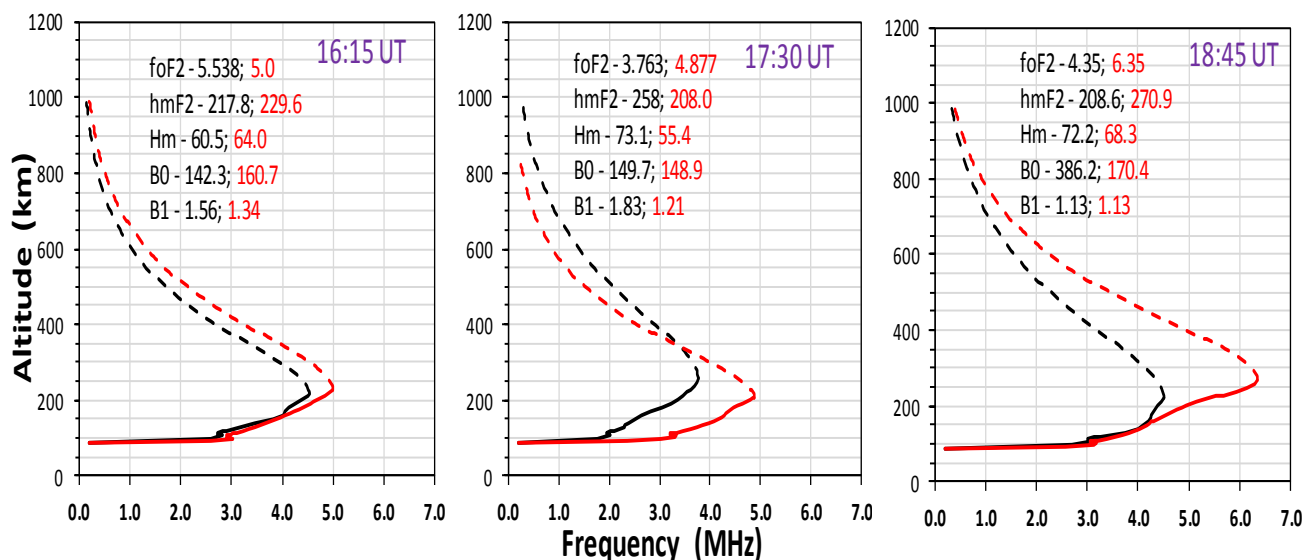


Figure 6: Example of the ionospheric profile at the eclipse window of Idaho National Lab showing the bottomside profile (continuous line) and the modelled topside profile shown as a dashed line. The black curve represents the profile for the eclipse day (August 21) and the red curve is for the one of the selected reference days, August 27. On the left side, was the profile during the first contact of the eclipse, the middle and the right profiles are for the maximum contact and the last contact of the eclipse respectively.